icct

THE INTERNATIONAL COUNCIL
ON CLEAN TRANSPORTATION

Rotors and bubbles: Route-based assessment of innovative technologies to reduce ship fuel consumption and emissions

Authors: Bryan Comer, Ph.D.[a]; Chen Chen, M.S.[a]; Doug Stolz, Ph.D.[b]; Dan Rutherford, Ph.D.[a]

1. Introduction

The International Maritime Organization (IMO), which regulates international shipping, has struggled with how to control greenhouse gas (GHG) emissions from ships since 1997, when the Kyoto Protocol to the United Nations Framework Convention on Climate Change tasked it with limiting or reducing GHG emissions. The IMO finally agreed, at the 72nd session of its Marine Environment Protection Committee (MEPC 72) in April 2018, to an initial strategy to reduce GHG emissions from ships. As summarized by Rutherford and Comer (2018), the initial strategy calls for improving the operational efficiency of international shipping, as an average across the fleet, by at least 40% by 2030, and aiming for a 70% improvement by 2050 (both percentages compared to 2008 levels). It also calls for at least a 50% reduction in GHG emissions from international shipping by 2050, compared to 2008 levels, and for the phase out of GHGs from the sector as soon as possible. Following the adoption of this initial strategy, attention is focusing on how to meet these targets. Accordingly, we examine two

underutilized technologies—wind-assist and hull air lubrication—that could help achieve the IMO's goals.

This is a preliminary, route-based analysis of fuel and emissions savings from wind-assist and hull air lubrication technologies for commercial ships. Our study integrates terrestrial and satellite Automatic Identification System (AIS) ship activity data with weather data for eight oceangoing vessels. Specifically, we model five ships that use rotor sails (also called Flettner rotors) and three ships that use hull air lubrication. We find that rotor sails can reduce route-level fuel consumption and emissions on the order of 1% to 12% per rotor. Air lubrication systems can reduce route-level fuel consumption and emissions by approximately 3%–13%, depending on draught and ship speed. Either technology can be incorporated into newbuild designs, and rotor sails can be retrofitted onto existing ships. Retrofitting would be especially helpful in reducing the carbon intensity of the existing fleet, and this can help achieve the IMO's operational efficiency targets while reducing fuel costs.

2. Background

In the early days of long-distance maritime shipping, wind power was the sole means of propulsion. Now, the sector relies on gigantic internal combustion engines that burn fossil fuels. The global shipping sector mostly burns residual fuels such as heavy fuel oil (72%); the other fuels are distillate (26%) and liquid natural gas (LNG; 2%), although a handful of commercial ships operate on nuclear power (these are mainly Russian ice-breakers) and several small ferries and tugs still use coal (Olmer, Comer, Roy, Mao, & Rutherford, 2017). In the wake of the 2008 global economic downturn, ship owners and operators sought ways to reduce fuel consumption to save on fuel costs, including by slowing down (slow steaming). As the global economy improves, some ships are starting to speed back up again (Olmer et al., 2017), and this will increase fuel use and GHG emissions.

To reduce emissions from the existing fleet, some advocates are calling for the IMO to regulate ship speeds as a short-term measure that can immediately reduce emissions, while

---

[a] International Council on Clean Transportation, [b] Cross Product Atmospheric

others suggest an operational efficiency standard to directly regulate the carbon intensity of ships (Comer, Chen, & Rutherford, 2018). Still others prefer a market-based measure (e.g., a carbon price) that seeks to control emissions by reducing demand for fossil fuels.

For new ships, the main tool to reduce emissions is the IMO's Energy Efficiency Design Index (EEDI) regulation, which requires new ships to be increasingly more efficient than older ships of similar type and size. Currently, the EEDI goes up to "phase 3," which generally requires that ships built in 2025 and beyond be 30% less carbon intensive in terms of carbon dioxide per deadweight tonne-nautical mile (g CO_2/dwt-nm) than a baseline of older ships. Phase 3 targets are expected to be made more stringent for some ship types, including container ships and general cargo ships, at the MEPC 74 meeting in May 2019.[1] To date, ship owners have complied with the EEDI mainly by building larger ships, installing smaller engines, or both. But compliance can also be achieved by using what the IMO calls "innovative technologies"; these include technologies that reduce the amount of power the ship needs from its engines by providing additional propulsion power (e.g., wind-assist) or reducing drag (e.g., hull air lubrication).

WIND-ASSIST TECHNOLOGIES

There are several wind-assist technologies available to ships, including traditional soft sails, rigid sails, suction wings, turbines, kites, and rotor sails (also called Flettner rotors). CE Delft (2016) predicted that wind-assist technologies could reduce CO_2 emissions between 3.5 million and 7.5 million tonnes in 2030. This would represent as much as a 0.8% reduction from business as usual emissions, according to projections of future international ship emissions from Rutherford and Comer (2018).

To be clear, wind-assist technologies are not yet widely used in the shipping sector. Rehmatulla, Parker, Smith, and Stulgis (2017) investigated the opportunities and barriers and found that while there is renewed interest in using wind-assist to save fuel, the potential technical risks, hidden costs, and lack of verifiable data on the fuel savings potential were key barriers. Nevertheless, wind-assist technologies have been installed on several ships already and there are plans to outfit several more ships with them in the future. Of the available wind-assist technologies, kites and rotor sails have received the most attention with respect to helping reduce fuel consumption and emissions from larger commercial ships.

Towing kites are deployed off the bow of a ship to harness the power of the higher-altitude winds, and they operate at an altitude of between 100

meters and 300 meters.[2] A handful of ships are using or have used kites, including the *Michael A.* general cargo ship, the *M/V Theseus* container/cargo ship, the *M/V BBC Skysails*, and the *Aghia Marina* bulk carrier. All of these ships use technology from SkySails, which claims a 10%–15% fuel saving potential and up to 2,000 kW of power generation on its website (www.skysails.info). Traut el al. (2014) estimated the power output of a towing kite would be between 127 kW and 461 kW in a case study of five potential trade routes. Depending on the ship, that could result in route-level power and fuel savings of 1% to 32%. Leloup et al. (2016) used an analytical model to evaluate kite performance as an auxiliary power source. A 320 m^2 kite on a 50,000 dwt tanker, for example, would achieve 10% fuel savings with a wind speed of 10 m/s and up to 50% savings at 15.6 m/s. Traut and colleagues (2014) noted that the performance of kites is more volatile than rotor sails, but still concluded that kites are a low-carbon solution that should continue to be considered.

Rotor sails are 18-to-30-meter tall vertical spinning columns that are installed on the deck of a ship. They are powered by small electric motors. As wind comes across the deck of the ship, the rotors generate forward thrust by using the Magnus effect, and this replaces or supplements a portion of the propulsion power the main engines would otherwise

---

1   At MEPC 73, the IMO tentatively agreed to require new container ships to be 40% less carbon intensive than the EEDI baseline by 2022, rather than 30% by 2025. Additionally, new general cargo ship carbon intensity would need to be 30% lower than baseline by 2022, rather than 2025. The actual phase 3 targets will be agreed at MEPC 74 in 2019. More information is available at https://www.theicct.org/blog/staff/imo-cargo-container-efficient.

2   Modeling the fuel savings potential of towing kites was beyond the scope of this analysis, but we briefly introduce the technology here because it is one solution that has been trialed on several ships. Our analysis focuses on rotor sails and air lubrication, but future work could expand to other wind-assist and drag reduction technologies.

provide.[3] Rotor sails have been used on several commercial ships in recent years, with one new build (the 63,000 dwt *Afros* bulk carrier) and at least three retrofits in 2018 alone, including the 2,800-passenger *Viking Grace* cruise ship, the 4,250 dwt *Fehn Pollux* general cargo ship, and the 110,000 dwt *Maersk Pelican* tanker vessel. One of the most famous ships with rotor sails is the *E-Ship 1* (Figure 1), which was purpose-built with four rotor sails in 2010 to transport wind turbine blades, towers, and equipment for German wind turbine manufacturer Enercon. Rotor sails can be retrofitted onto an existing ship and can be designed to move out of the way or retract during loading and unloading.

Figure 1. The E-Ship 1 cargo ship with four rotor sails sailing near Aberdeenshire, Scotland in 2015. *Photo Credit: "E-Ship 1" by Alan Jamieson is licensed under CC BY 2.0: https://bit. ly/2vbIcYF*

By applying a numerical model, Traut et al. (2012) estimated that up to 16% fuel savings are possible for a typical bulk carrier equipped with three Flettner rotors along a route from Tubarao (Brazil) to Grimsby (UK). That is about 5.3% per rotor. Later, Traut and colleagues (2014) modeled additional routes in five case studies and found the average of wind power contribution was in the range of 193 kW to 373 kW per rotor, the equivalent of 2%–24% fuel savings for a typical ship. Pearson (2014) used a software model to assess the viability of installing Flettner rotors on ships and estimated up to 10% annual fuel savings per rotor for a 14,700 dwt chemical tanker. De Marco, Mancini, Pensa, Calise, and De Luca (2016) concluded that two Flettner rotors could provide up to 30% of propulsion power needs for a 75,000 dwt product tanker. Finally, Talluri, Nalianda, and Giuliani (2018) claimed that rotor sails could

achieve up to 20% fuel savings for commercial cargo ships, assuming three rotors were installed.

HULL AIR LUBRICATION TECHNOLOGIES

Air lubrication systems work by reducing drag force between the ship's hull and the surrounding water. A blower pumps air bubbles beneath the ship, covering a portion of the hull; this reduces resistance, and thereby reduces the amount of power the main engines need to provide to maintain a given speed. Of the few ships that have air lubrication systems, most use the Mitsubishi Air Lubrication System (MALS). However, a couple of cruise ships—the *Norwegian Joy* and the *Norwegian Bliss*—use a system called Silverstream. To our knowledge, these technologies have thus far only been installed on newbuild ships, and there are no retrofits.

Latorre (1997) found that air lubrication reduced drag 10%–12% for a river barge. Later, Latorre, Miller, and Philips (2003) reported a 5%–11% drag reduction from micro-bubbles for a

high-speed catamaran. Thill, Toxopeus, and van Walree (2005) modeled the drag reduction potential of air lubrication in the laboratory and found it could reduce power demand from 3% to 10% in calm waters. Thill et al. (2005) explained that the model prototype itself is only a ship-like shape and that better real-world performance could likely be achieved through implementing actual design strategies. Mäkiharju, Perlin, and Ceccio (2012) modeled the *M/V American Spirit* bulk carrier, currently operating on the North American Great Lakes, and determined that air lubrication could reduce fuel consumption by 10% to 20% for these types of lakers which have large, flat bottoms. With respect to the MALS system, Mizokami et al. (2010) found that MALS can deliver 8%–12% drag reduction in a sea trial of the *Yamatai* general cargo ship, one of the ships we model in this analysis.

3. Methodology

This section describes the ships we modeled and our basic approach. A detailed description of the methodology used to calculate the

---

3 This 2017 *Science* magazine article explains how rotor sails use the Magnus effect to generate lift and, therefore, propulsion power for ships: https://www.sciencemag.org/news/2017/09/spinning-metal-sails-could-slash-fuel-consumption-emissions-cargo-ships

fuel-use-reduction potentials of wind-assist and hull air lubrication systems is in the appendix. These fuel-consumption reductions were used to calculate CO_2 and carbon-intensity reductions.

We modeled five ships with rotor sails (Table 1) and three ships with hull air lubrication systems (Table 2). We chose ships that had wind-assist or hull air lubrication systems installed as of 2018 that were also operating in 2015. The International Council on Clean Transportation (ICCT) has global AIS ship traffic data and global meteorological data (atmospheric pressure, wind speed, wind direction, etc.) for the year 2015, so we were able to model real-world voyages and estimate potential energy and fuel savings of these ships along these routes. To be clear, three of the rotor ships (*Viking Grace*, *Fehn Pollux*, and *Maersk Pelican*) did not have rotor sails installed in 2015; they were retrofitted in 2018. However, these ships are included in our 2015 AIS data and we were able to model potential energy and fuel savings for them along these routes, as if the technology had been installed. It is possible that after the rotor sails were installed, these three ships changed their behavior to take advantage of more favorable routes; future work could explore if this was the case. For the other ships, though, our analysis reflects the actual routes these ships sailed while the technology was installed.

The *E-Ship 1* is a ~10,000 dwt general cargo ship owned by Enercon, a German wind turbine manufacturer.

The ship uses four rotor sails, more than any other ship to date. It primarily transports Enercon's wind turbines. Fuel savings of up to 25%, depending on weather conditions, are advertised (Enercon, 2013), although recent *E-Ship 1* press stemming from the ship's class renewal reports 15% (Wind Business Intelligence, 2018).

The *Estraden* is a ~9,700 dwt roll-on/roll-off (ro-ro) carrier owned by Finnish company Bore Ltd. The ship uses two Norsepower rotor sails and conducts routine service between the Netherlands and the United Kingdom (UK). Sea trials showed a 2.6% fuel savings when using one small rotor sail (Bore Ltd., 2015). After installing a second rotor sail, sea trials revealed a 6.1% fuel savings (Blenkey, 2016).

The 2,800-passenger, LNG-fueled *Viking Grace* is the world's first passenger ship equipped with a rotor sail. Viking Line says the rotor will allow the *Grace* to save up to 900 tonnes of CO_2 annually on the runs between Turku, Finland, and Stockholm, Sweden (Lloyds Register, 2018). According to ICCT data produced while developing a global shipping emissions inventory (Olmer et al., 2017), the *Viking Grace* burned 23,500 tonnes of LNG in 2015, emitting about 53,000 tonnes of CO_2 in the process; therefore, a 900-tonne reduction in CO_2 is equivalent to a 1.7% reduction in emissions and fuel consumption. Recently, Viking Line announced that a cruise ferry currently under construction in China will receive two Norsepower rotor sails (The Maritime Executive, 2018).

The *Fehn Pollux* general cargo ship installed a Flettner rotor system, called the EcoFlettner, in 2018. The EcoFlettner is an 18-m high, 3-m diameter rotor. While public data on performance are not available, researchers who conducted a sea trial of the rotor system on the *Fehn Pollux* claimed that, "in perfect conditions, this prototype will deliver more thrust than the main engine" (MariGreen, 2018, para. 1).

In 2018, when the *Maersk Pelican* installed two Norsepower rotor sails, it became the first tanker ship to use a wind-assist technology (Maersk Tankers, 2018). The rotors on the *Maersk Pelican* are taller and thicker than those on the *Estraden* or *Viking Grace*, at 30 m high and 5 m in diameter. The rotor sails are expected to reduce fuel consumption and associated emissions from the *Pelican* by about 7%–10% (Chan, 2018).

Table 2 summarizes the air-lubrication systems analyzed in this study. In April 2010, Japan's Mitsubishi Heavy Industries (MHI) finished building the *Yamatai*, a 14,500 dwt Panama-flagged general cargo ship that was the first to use the MALS system. Several months later, in December 2010, HMI launched a sister ship named the *Yamato*, which is also equipped with the MALS system. The *Yamatai* achieved between 8% and 12% fuel savings in sea trials, depending on the thickness of air lubrication (Mizokami

Table 1. Wind-assist ships analyzed.

Ship name	Ship type	Capacity	Number of rotors	Diameter of rotors (m)	Height of rotors (m)	Ship Build year	Rotor installation year
E-Ship 1	General cargo/Ro-Lo	10,020 dwt	4	4	27	2010	2010
Estraden	Ro-Ro	9,700 dwt	2	4	18	1999	2014
Viking Grace	Passenger	2,800 pax	1	4	24	2013	2018
Fehn Pollux	General cargo	4,250 dwt	1	3	18	1997	2018
Maersk Pelican	Tanker	109,647 dwt	2	5	30	2008	2018

et al., 2010), and the *Yamato* sister ship is expected to achieve similar results.

The *Soyo* is a 92,000 dwt bulk carrier (more than five-times the size of the *Yamatai* and *Yamato*). The *Soyo* was built in 2012 and typically transports Australian coal to power stations in eastern Japan. In the *Soyo*'s sea trials, the MALS system delivered 8.1% fuel and emissions reductions under normal ballast conditions (6.6 m draught) and 4.4% under heavy ballast (8.8 m draught). On the ship's maiden voyage, tests confirmed fuel savings, albeit smaller than the sea trials: 5% under heavy ballast conditions and 3% when loaded (Oshima Shipbuilding Co. Ltd., 2014).

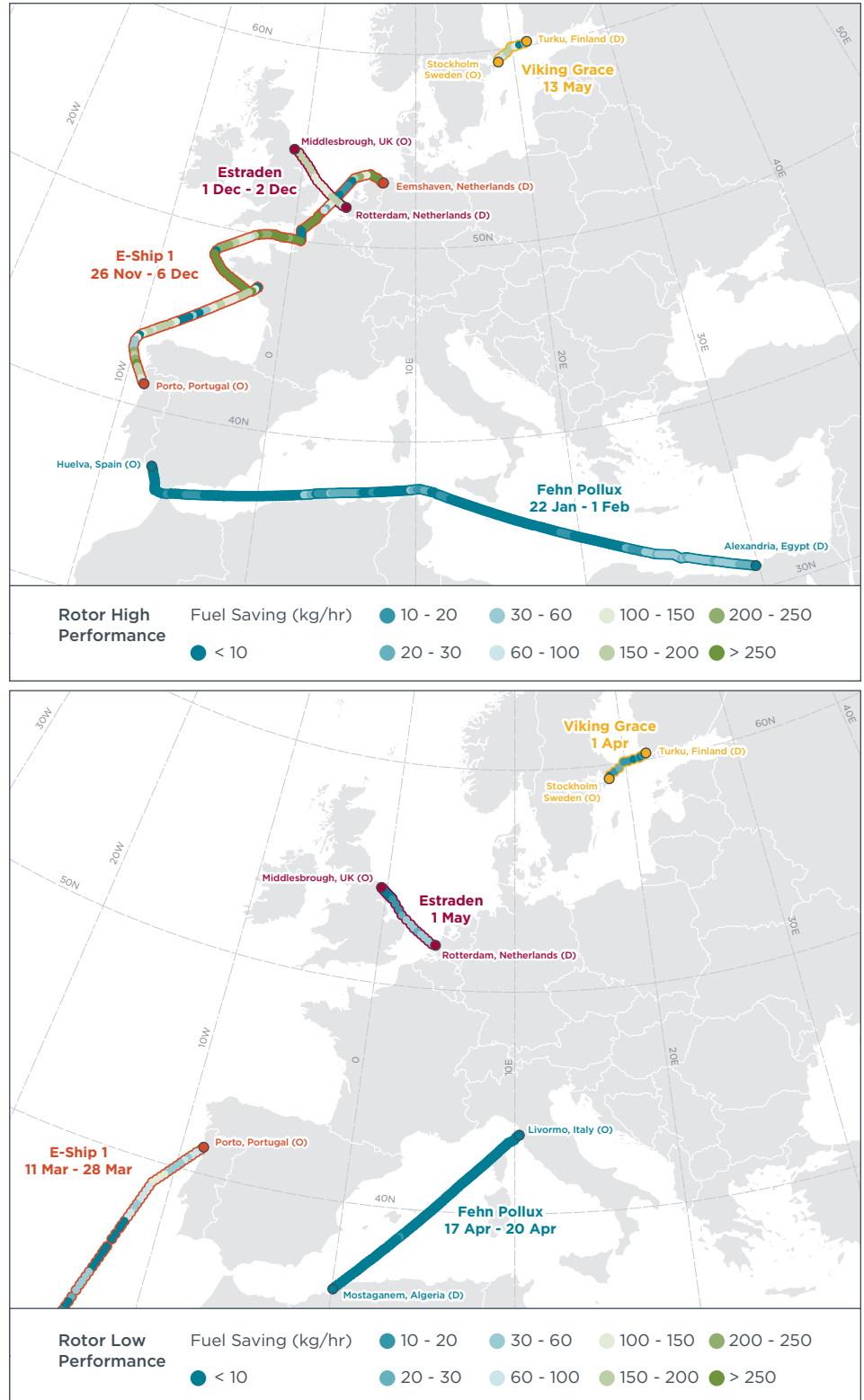**Table 2.** Air-lubrication (MALS) ships analyzed.

Ship name	Ship Type	Capacity (dwt)	Ship build year	Air lubrication installation year
Yamatai	General cargo	14,538	2010	2010
Yamato	General cargo	14,538	2010	2010
Soyo	Bulk carrier	91,867	2012	2012

4. Results and Discussion

This section describes the range of fuel use, emissions, and carbon-intensity reductions for five ships using wind-assist (rotor sails) technologies and three that use hull air lubrication technology (MALS).

WIND-ASSIST (ROTOR SAILS)

We modeled fuel consumption without and with rotor sails. We report two routes—one representing low fuel savings and one representing high fuel savings (Table 3). We also mapped these routes (Figure 2 and Figure 3). Figure 2, which zooms in

Figure 2. Modeled fuel savings per hour for high-performance (top) and low-performance (bottom) routes for four ships using rotor sails near Europe; (O) represents origin and (D) destination.

on a geographical area surrounding Europe, shows fuel savings for four of the five ships that have rotor sails. The top panel shows the high-performance route for each ship and the bottom panel shows the low-performance route. The global map in Figure 3 shows all five ships, including the *Maersk Pelican* tanker, which traveled between Asia and Europe via the Suez Canal. Table 3 provides more details on route-level results for all five ships.

Depending on the ship and the route, rotor sails could save tens to hundreds of kilograms of fuel per hour, representing route-level fuel savings ranging from less than 1% to nearly 50% and per-rotor fuel savings of approximately 1% to 12%. The greatest absolute fuel savings were observed off the western coast of Europe, in the South China Sea, the Indian Ocean, and the Arabian Sea, while the smallest savings occurred in the Mediterranean Sea and off the west coast of Africa (Figure 3). Smaller savings were also observed in the spring in the Northern Hemisphere. Larger fuel and emissions savings were observed in the winter, when wind speeds tend to be higher in the Northern Hemisphere than other times of the year.

As Table 3 shows, in each case, the high-performance route had substantially higher average wind speed at 30 m than the low-performance route. This is unsurprising, given that rotor sail performance depends on wind speed and direction. When the wind is across the beam and strong, it results in higher fuel savings than times with a headwind or when the wind speed is slower. That said, greater wind speeds can also generate larger waves that can increase the hydrodynamic forces on the ship and increase fuel consumption. Wind also increases aerodynamic drag. The ICCT's Systematic Assessment of Vessel Emissions (SAVE) model, described in Olmer et al. (2017), includes a weather adjustment factor consistent with
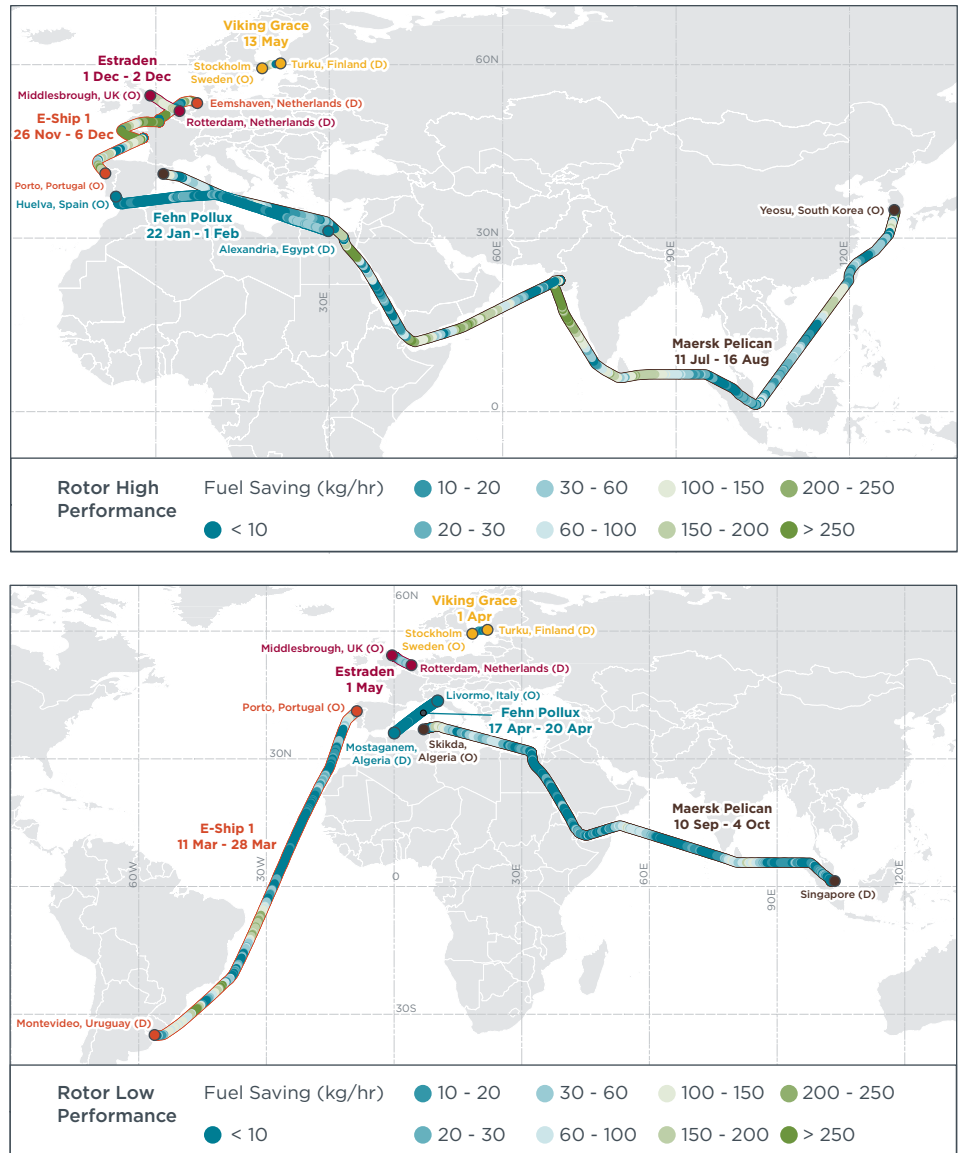
Figure 3. Modeled fuel savings per hour for high-performance (top) and low-performance (bottom) routes for five ships using rotor sails globally; (O) represents origin and (D) destination.

the Third IMO GHG Study 2014. The weather adjustment factor increases the main engine fuel power demand to account for the additional power needed to overcome resistance from wind and waves. When the ship is within five nautical miles from shore, the weather adjustment factor increases main engine power demand by 10%, and when the ship is greater than five nautical miles from shore, the adjustment factor increases main engine

power demand by 15%. As such, we have taken wind and wave effects into account in a simple way; however, future work could develop a more sophisticated approach to incorporate the impact of waves into the modeling.

In some cases, the fuel savings we modeled for these voyages fall short of claimed route-level savings, and in others, they exceed them. Quoted performance generally fit well within the range of the low and high performance

Table 3. Rotor sail performance

Ship name	Routes: Low (L) and high (H) performance	Distance travelled (nm)	Average wind speed (kts) at 30 m[a]	Fuel consumed w/o rotors (tonnes)	Fuel savings along route (tonnes)	CO_2 savings along route (tonnes)	Fuel, CO_2, or carbon-intensity savings along route and per rotor (r)	Claimed route-level fuel savings
E-Ship 1	L: Portugal to Uruguay 11-28 Mar	5,404	12.1	272	23	70	8.3% (2.1%/r)	15%–25%[b]
	H: Netherlands to Portugal 26 Nov-6 Dec	1,407	19.8	50	23	73	47% (11.8%/r)	
Estraden	L: UK to Netherlands 1 May	218	17.2	25	0.5	1.3	1.6% (0.8%/r)	6.1%[c]
	H: UK to Netherlands 1–2 Dec	246	22.3	30	2.7	8.3	9.0% (4.5%/r)	
Viking Grace	L: Sweden to Finland 1 Apr	145	4.4	36	0.1	0.4	0.40% (0.40%/r)	About 1.7% per year[d]
	H: Sweden to Finland 13 May	138	10.9	39	1.1	3.0	2.8% (2.8%/r)	
Fehn Pollux	L: Italy to Algeria 17-20 Apr	656	8.1	18	0.2	0.6	1.0% (1.0%/r)	100% in "perfect conditions"[e] but no data reported
	H: Spain to Egypt 22 Jan-1 Feb	1,929	17.1	47	3.1	9.7	6.6% (6.6%/r)	
Maersk Pelican	L: Algeria to Singapore 10 Sept-4 Oct	6,426	8.1	812	15	46	1.8% (0.9%/r)	7–10%[f]
	H: South Korea to Spain 11 Jul-16 Aug	9,893	14.4	1,399	66	206	4.7% (2.4%/r)	

[a] Proxy for wind speed the rotor would encounter; [b] Enercon (2013) and Wind Business Intelligence (2018); [c] Blenkey (2016); [d] Lloyds Register (2018) and ICCT data from Olmer et al. (2017); [e] MariGreen (2018); [f] Chan (2018)

routes shown in Table 3. The *E-Ship 1* low-performance route realized 8% fuel savings and the high-performance route resulted in 47% savings, compared to claims of 15% to 25%. This reflects 2% to roughly 12% fuel and emissions savings per rotor. The *Estraden* saw 1.6% to 9% savings versus 6.1% claims. The *Viking Grace* saved between 0.40% and 2.8%, compared with estimated annual fuel savings of 1.7%. The *Fehn Pollux* saved between 1% and 6.6%; it is difficult to know how that value compares to expected results, given that sea trial results have

not been reported for this ship. The *Maersk Pelican* fell short of industry claims in terms of percent-fuel-use reduction, with roughly 2%–5% route-level savings, or approximately 1% to 2.5% per rotor. Nevertheless, the *Pelican* realized substantial fuel savings—about 200 tonnes of fuel—that is equivalent to more than 600 tonnes of CO_2, in the higher performance route.

Finally, as expected, using multiple rotors seems to increase fuel savings. The *E-Ship 1*, with its four rotors, met

nearly half of its energy demand using wind-assist in our model. The *Estraden* is similar in shape and size to the *E-Ship 1*, but with two rotors, its high-performance route (9% savings) is only marginally better than the *E-Ship 1*'s low-performance route (8.3% savings). There are tradeoffs, though, because adding additional rotors uses up valuable deck space, requires upfront capital investment, and results in additional operating and maintenance costs. Nevertheless, we show that multiple rotors can deliver fuel and emissions-reduction benefits.

HULL AIR LUBRICATION

We modeled fuel consumption without and with air lubrication (MALS). We modeled the routes of three ships – the *Yamatai* and *Yamato* general cargo ships and the *Soyo* bulk carrier. Results are shown in Figure 4, with detailed results in Table 4. Note that the *Yamato* and *Yamatai* routes overlap each other, so we map one low performance route for the *Yamato* and one high- performance route for the *Yamatai* in Figure 4; however, we include complete results for both ships in Table 4.

We find that using MALS can save about 12% to 13% on fuel consumption along each route for the two sister general cargo ships, *Yamatai* and *Yamato*. The modeled performance

for these ships under the low-performance and high-performance scenarios was quite similar because ship speed and draught are the main driver of MALS performance in the model. The draught was 4.5 m for each ship for each route, and with increased ship speed came increased fuel savings, as expected. We assumed that the ships were loaded when traveling along these routes.

For the *Soyo* bulk carrier, we observed more than 3% fuel savings under loaded conditions but nearly 12% fuel savings under ballast. This finding was expected, especially because the *Soyo* has a large difference in draught between loaded (12.8 m) and ballast (7.5 m) conditions. When the ship is

under ballast, less of the ship is underwater, and this reduces hydrodynamic drag forces. Additionally, blower energy use is lower under ballast because it takes less power to expel the air bubbles when the bottom hull is shallower in the water.

Like the rotor-sail results, MALS performance will depend on environmental conditions such as surface pressure and waves. These effects of weather on energy use, fuel consumption, and emissions are accounted for in a simple way in the SAVE model, as explained in the rotor-sail results subsection. However, more sophisticated approaches to modeling the impacts of weather on ship performance could be integrated in future work.
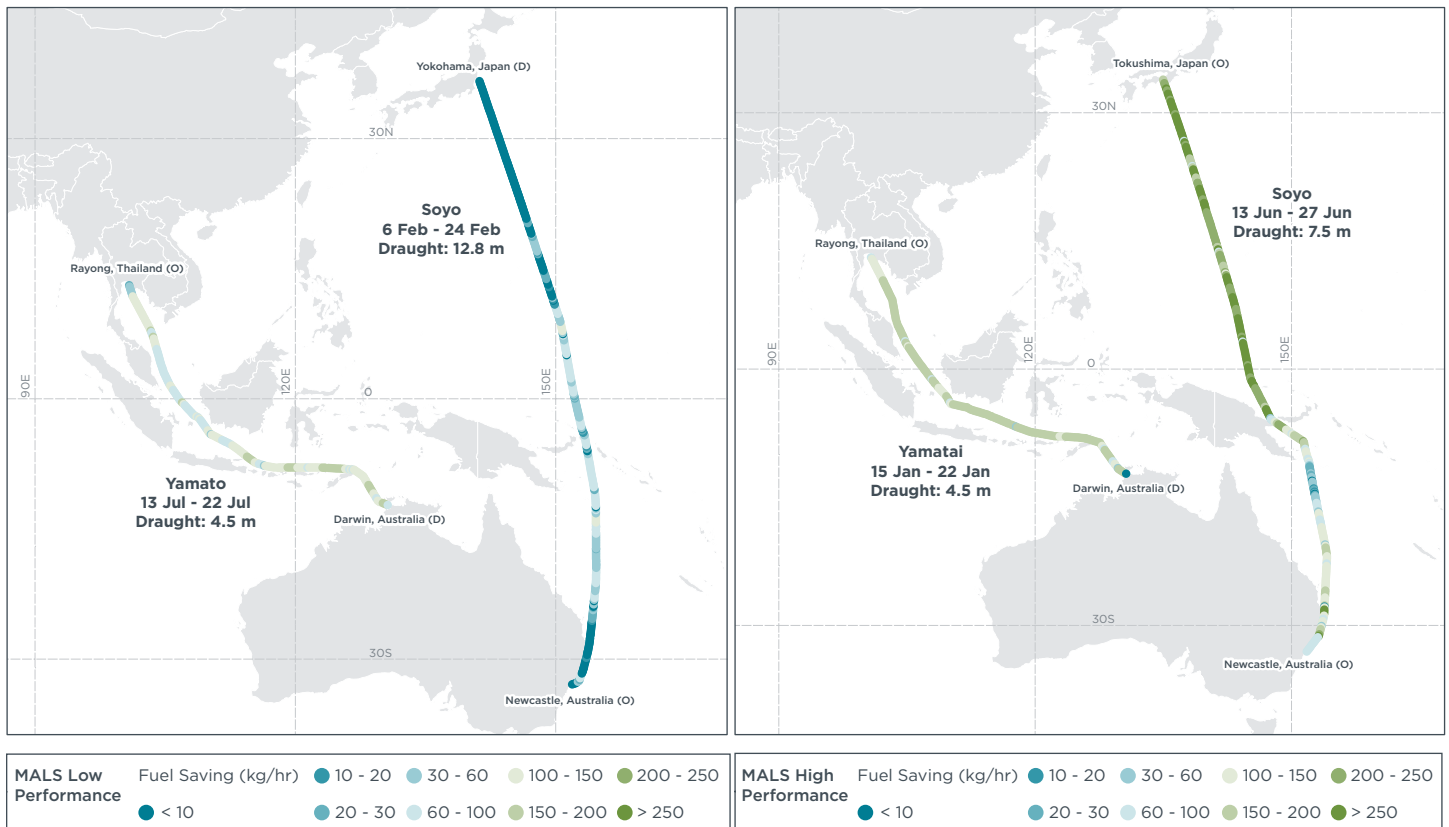
Figure 4. Modeled fuel savings per hour for low-performance (left) and high-performance (right) routes for three ships using air lubrication systems; (O) represents origin and (D) destination.

Table 4. Air lubrication performance

Ship name	Routes: Low (L) and High (H) performance	Distance travelled (nm)	Average ship speed (kts)	Fuel consumed w/o air lubrication (tonnes)	Fuel savings along route (tonnes)	CO_2 savings along route (tonnes)	Fuel, CO_2, or carbon-intensity savings along route	Manufacturer fuel savings claims
Yamatai	L: Australia to Thailand 17-26 Sept	2,592	12.3	194	24	75	12.4%	8–12%[a]
	H: Thailand to Australia 15-22 Jan	2,560	13.9	230	30	93	13.0%	
Yamato	Thailand to Australia 13-22 Jul	2,594	12.1	194	24	74	12.3%	8–12%[a]
	Thailand to Australia 23-31 Mar	2,624	12.8	215	27	85	12.7%	
Soyo	L: Australia to Japan (loaded) 6-24 Feb	4,319	10.0	358	12	38	3.4%	3%–4.4% when loaded[b]
	H: Japan to Australia (ballast) 7-17 Mar	4,304	12.3	533	63	196	11.8%	5%–8% under ballast[b]

[a] Mizokami et al. (2010); [b] Oshima Shipbuilding Co. Ltd. (2014)

CARBON INTENSITY

The carbon intensity varies from ship to ship (Figure 5). Larger ships, such as the *Maersk Pelican* tanker and the *Soyo* bulk carrier, have low carbon intensities when measured in terms of CO_2/dwt-nm because they can carry large quantities of bulk cargo at once. Smaller ships, such as the *Estraden* ro-ro ship, are relatively more carbon intensive. In this case, the higher carbon intensity is mainly because its cargo (i.e., vehicles) takes up a relatively large volume for relatively low weight compared to liquid bulk cargo vessels such as tankers and dry bulk cargo vessels such as bulk carriers. Despite the differences in absolute carbon intensities, each ship becomes less carbon intensive when using the rotor sail technologies (the first five ships in Figure 5) or the air lubrication technologies (the last three ships in Figure 5). The percentage of carbon intensity reduction is reported in Table 3 for ships using rotor sails and Table 4 for ships using air lubrication. We note that large ships that already have relatively low carbon intensities, such as the *Maersk Pelican* (~110,000 dwt) and the *Soyo* (~92,000 dwt), may not have the largest fuel and emissions

savings expressed as a percentage, but they still save substantial absolute quantities of fuel and emissions along their routes. Even small improvements in fuel savings on large ships are beneficial, as they can help reduce both the overall carbon intensity of the existing fleet and the absolute emissions from the international shipping sector in general.

5. Conclusions

This preliminary assessment, which combined hourly AIS and global meteorological data, shows how innovative technologies such as wind-assist and air lubrication can reduce emissions from ships. For the ships and routes modeled, we found that rotor sails can reduce fuel consumption, CO_2 emissions, and ship-level carbon-intensity between approximately 1% and 47% (about 1% to 12% per rotor); air lubrication systems can yield savings of between 3% and 13%.

Rotor sail performance depends largely on wind speed and direction, and strong winds across the ship's beam generate the most power. In all cases, we found that rotor sails reduced route-level fuel consumption,

CO_2 emissions, and carbon intensity, although the magnitude depended on the type of ship, route, and associated weather conditions. In the Northern Hemisphere, we observed better performance in the winter months, when wind speeds tend to be stronger. We also saw a clear benefit to using multiple rotor sails, although additional rotors use more deck space. Ship owners who are interested in wind-assist technologies should consider the regions and typical weather conditions in which the ship operates, and should consider installing multiple rotors, when possible. Depending on fuel price, the payback period could be attractive.

Air lubrication fuel and emissions reduction potential depends mainly on draught and ship speed. Low draught and high ship speed result in better MALS performance, although faster ship speeds increase absolute route-level fuel consumption compared to slower speeds. Air lubrication performance is less sensitive to geography and provides more consistent fuel savings in the cases we modeled. Retrofitting air lubrication systems is uncommon to date, however, and thus

this technology may be better suited for newbuilds.

Putting these results in a broader policy context, these innovative technologies can be used to help reduce emissions from existing and new ships in a way that helps the IMO achieve the ambitions of its initial GHG strategy. Using wind-assist and/or hull air lubrication reduces the carbon-intensity of the ship and, on a large enough scale, will reduce the carbon-intensity of maritime shipping overall and reduce absolute emissions from the sector.

Wind-assist and hull air lubrication can also help comply with increasingly more stringent EEDI regulations, as ships receive credit for installing and operating innovative technologies that reduce fuel consumption. Given that ships often remain in service for 20 to 30 years or longer, installing these technologies on newbuilds today will reduce emissions now and for decades into the future.

These technologies also reduce the overall energy needed to complete a voyage. As ships start using alternatives to fossil fuels, ships that are more efficient will be more competitive in the sector. This is crucial because sustainable biofuels, electricity, hydrogen, and other fuels will be both limited in supply and costly, especially in the near term. Wind-assist and air lubrication technologies can make it easier for new ships to operate on low- and
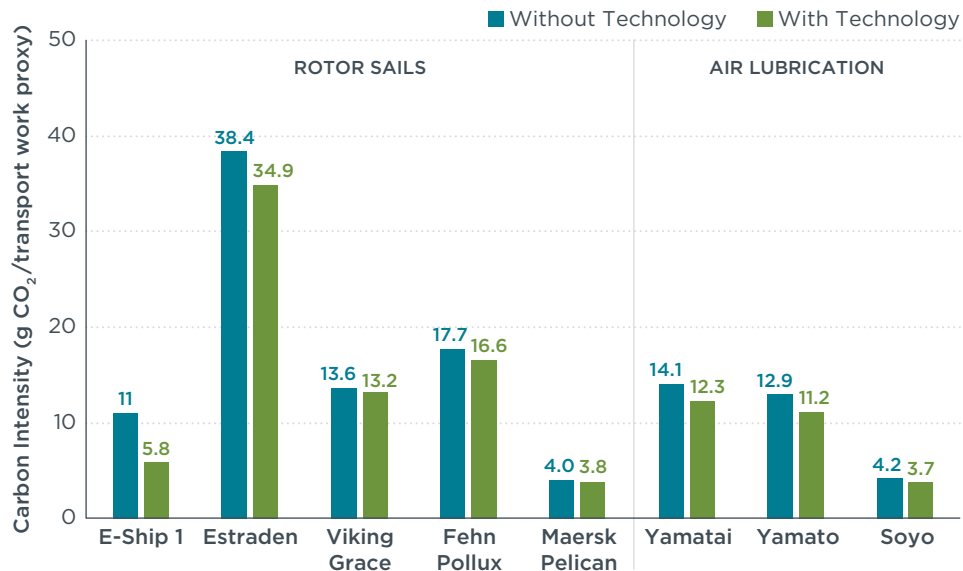
Figure 5. Carbon intensity change after applying rotor sails (first five ships) or air lubrication (last three ships) for the high-performance scenarios. Note: transport work is deadweight-tonne-nautical miles for all ships except the *Viking Grace*, which is gross-tonne-nautical miles.

zero-carbon fuels and energy. This will help the IMO achieve its minimum 2050 emissions reduction goal as well as its ultimate goal of completely eliminating GHG emissions from the sector as soon as possible.

Future work could include refining the model to better account for the influence of weather factors that can affect energy demand, examining additional routes and multiple years, and expanding the analysis to a larger portion of the global shipping fleet. There is also the opportunity to model the combined impacts of using wind-assist and air lubrication

systems together, and to estimate the range of payback periods for wind-assist and hull air lubrication technologies, especially after 2020, when the IMO's global maximum 0.5% fuel sulfur content standard begins. Such additional analyses would help illuminate the potential of these innovative technologies to reduce emissions from the international shipping sector. They are among the many tools capable of reducing the carbon intensity of the sector, improving vessel efficiency, and supporting a transition to low- and zero-carbon fuels and propulsion technologies.

References

Blenkey, N. (2016, August 25). Norsepower gets new funding for Rotor Sail development. *MarineLog*. Retrieved from https://www.marinelog.com/news/norsepower-gets-new-funding-for-rotor-sail-development/.

Bore Ltd. (2015). *Successful trial-phases for Norsepower's Rotor Sail System onboard M/V Estraden.* Retrieved from https://www.bore.eu/successful-trial-phases-for-norsepowers-rotor-sail-system-onboard-mv-estraden/.

CE Delft. (2016). *Study on the analysis of market potentials and market barriers for wind propulsion technologies for ships.* Retrieved from https://www.cedelft.eu/publicatie/study_on_the_analysis_of_market_potentials_and_market_barriers_for_wind_propulsion_technologies_for_ships/1891.

Chan, K. (2018, December 9). Answer's a breeze in shippers' clean-energy quest. *Associated Press*. Retrieved from https://www.arkansasonline.com/news/2018/dec/09/answer-s-a-breeze-in-shippers-clean-ene/.

Comer, B., Chen, C., & Rutherford, D. (2018). *Relating short-term measures to IMO's minimum 2050 emissions reduction target*. International Council on Clean Transportation. Retrieved from https://www.theicct.org/publications/short-term-measures-IMO-emissions.

De Marco, A., Mancini, S., Pensa, C., Calise, G., & De Luca, F. (2016). Flettner rotor concept for marine applications: A systematic study. *International Journal of Rotating Machinery* (2016). http://dx.doi.org/10.1155/2016/3458750.

Enercon GmbH (2013). *Rotor sail ship E-Ship 1 saves up to 25% fuel.* Retrieved from https://www.evwind.es/2013/07/30/enercon-rotor-sail-ship-e-ship-1-saves-up-to-25-fuel/34733.

Latorre, R. (1997). Ship hull drag reduction using bottom air injection. *Ocean Engineering, 24*(2), 161–175. https://doi.org/10.1016/0029-8018(96)00005-4.

Latorre, R., Miller, A., & Philips, R. (2003). Micro-bubble resistance reduction on a model SES catamaran. *Ocean Engineering, 30*(17), 2297-2309. https://doi.org/10.1016/S0029-8018(03)00079-9.

Leloup, R., Roncin, K., Behrel, M., Bles, G., Leroux, J.-B., Jochum, C., & Parlier, Y. (2016). A continuous and analytical modeling for kites as auxiliary propulsion devoted to merchant ships, including fuel saving estimation. *Renewable Energy, 86*, 483–496. https://doi.org/10.1016/j.renene.2015.08.036

Lloyds Register. (2018). Viking Grace installs rotor sail for wind-assisted propulsion. Retrieved from https://www.lr.org/en/latest-news/viking-grace-installs-rotor-sail/.

Maersk Tankers. (2018). *Testing begins on first product tanker vessel utilising wind propulsion technology.* Retrieved from https://maersktankers.com/media/testing-begins-on-first-product-tanker-vessel-utilising-wind-propulsion-technology.

Mäkiharju, S. A., Perlin, M., & Ceccio, S. L. (2012). On the energy economics of air lubrication drag reduction. *International Journal of Naval Architecture and Ocean Engineering*, 4(4), 412–422. https://doi.org/10.2478/IJNAOE-2013-0107.

MariGreen. (2018, December 6). *Investment into Flettner-rotor pays off.* Retrieved from http://en.marigreen.eu/ecoflettner-installation/.

Mizokami, S., Kawakita, C., Kodan, Y., Takano, S., Higasa, S., & Shigenaga, R. (2010). Experimental study of air lubrication method and verification of effects on actual hull by means of sea trial. *Mitsubishi Heavy Industries Technical Review, 47*(3), 41-47. Retrieved from https://www.mhi.co.jp/technology/review/pdf/e473/e473041.pdf.

Olmer, N., Comer, B., Roy, B., Mao, X., & Rutherford, D. (2017). *Greenhouse gas emissions from global shipping, 2013–2015.* International Council on Clean Transportation. Retrieved from https://www.theicct.org/publications/GHG-emissions-global-shipping-2013-2015.

Oshima Shipbuilding Co., Ltd. (2014). *Energy saving by air bubbles air lubrication technology applied to M.V. SOYO.* Retrieved from https://www.monohakobi.com/en/wp-content/uploads/2015/04/Energy_saving_by_air_bubbles_001039004.pdf.

Pearson. D. R. (2014) *The use of Flettner rotors in efficient ship design*. Influence of EEDI on Ship Design, 24-25 September, 2014. London, UK. Royal Institution of Naval Architects. Retrieved from https://www.semanticscholar.org/paper/THE-USE-OF-FLETTNER-ROTORS-IN-EFFICIENT-SHIP-DESIGN-Pearson/641a95be34ec48240aefab3700e2ac13fe67a4ac.

Rehmatulla, N., Parker, S., Smith, T., & Stulgis, V. (2017). Wind technologies: Opportunities and barriers to a low carbon shipping industry. *Marine Policy, 75*, 217–226. https://doi.org/10.1016/j.marpol.2015.12.021.

Rutherford, D., & Comer, B. (2018). *The International Maritime Organization's initial greenhouse gas strategy.* International Council on Clean Transportation. Retrieved from https://www.theicct.org/publications/IMO-initial-GHG-strategy.

Talluri, L., Nalianda, D.K., & Giuliani, E. (2018). Techno economic and environmental assessment of Flettner rotors for marine propulsion. *Ocean Engineering, 154*, 1-15. https://doi.org/10.1016/j.oceaneng.2018.02.020.

The Maritime Executive (2018, April 11). Viking Line installs rotor sails on cruise ferry. Retrieved from https://www.maritime-executive.com/article/viking-line-installs-rotor-sail-on-cruise-ferry.

Thill, C., Toxopeus, S., & van Walree, F. (2005). Project energy-saving air-lubricated ships (PELS). In: Proceedings of the Second International Symposium on Seawater Drag Reduction, Busan, Korea. Retrieved from http://www.marin.nl/upload_mm/f/a/1/1807359053_1999999096_ISSDR2005-Thill-Toxopeus-Walree-Project_Energy-saving_air-Lubricated_Ships.pdf

Traut, M., Bows, A., Gilbert, P., Mander, S., Stansby, P., Walsh, C., & Wood, R. (2012). *Low C for the High Seas Flettner rotor power contribution on a route Brazil to UK*. Second International Workshop on Successful Strategies in Supply Chain Management Template. Retrieved from https://www.researchgate.net/publication/233863726_Low_C_for_the_High_Seas_Flettner_rotor_power_contribution_on_a_route_Brazil_to_UK.

Traut, M., Gilbert, P., Walsh, C., Bows, A., Filippone, A., Stansby, P., & Wood, R. (2014). Propulsive power contribution of a kite and a Flettner rotor on selected shipping routes. *Applied Energy, 113*, 362–372. https://doi.org/10.1016/j.apenergy.2013.07.026.

Wind Business Intelligence. (2018). *Class renewal for the 'E-Ship 1'*. Retrieved from https://www.windbusinessintelligence.com/news/class-renewal-%E2%80%98e-ship-1%E2%80%99.

Appendix: Detailed methodology

This appendix explains how we incorporated meteorological data with ship activity data to estimate route-level fuel, carbon dioxide (CO_2), and carbon-intensity savings for ships using wind-assist (rotor sails) and air lubrication (Mitsubishi Air Lubrication System, or MALS) technologies. First, we explain how we obtained the meteorological data used in the calculations. Then we explain how we estimated the route-level fuel savings for each technology (rotor sails and air lubrication) by combining the meteorological and ship activity data sets.

METEOROLOGICAL DATA

The rotor sail methodology incorporates true wind speed (V_t) and wind direction (γ). These variables were estimated at points around the world using reanalysis weather data, which is based on input from routine surface- and space-based atmospheric/oceanic observation systems (Dee, Fasullo, Shea, & Walsh, 2016). Specifically, reanalysis is a method to collect and assimilate all such available observations from disparate local and remote-sensing platforms (i.e., from oceangoing vessels, ocean buoys, aircraft reports, surface stations, weather balloons and satellites, etc.) and to routinely aggregate them into a unified data framework for research and operational applications. Reanalysis was developed in the late 1970's and early 1980's, and today many agencies worldwide have created their own global reanalysis products (e.g., the United States National Oceanographic and Atmospheric Administration's National Center for Environmental Prediction [NCEP] and the Japanese Meteorological Agency [JMA]). Data characterizing the environmental weather conditions (e.g., wind, temperature, and atmospheric pressure) for the current study are derived from an atmospheric reanalysis model originally developed by the European Centre for Medium-Range Weather Forecasts (ECMWF)—the ERA-Interim Reanalysis (ERAi; Berrisford et al., 2011; Dee et al., 2011). The ERAi reanalysis is specifically regarded as a superior representation of near-surface wind speed characteristics, for reasons that are beyond the scope of this report (Decker et al., 2012).

The viability of individual data streams for long-term investigations (i.e., studies encompassing one year or longer) is subject to instrument malfunction, localized coverage, and intermittent reporting, whereas modern reanalysis products can now realistically provide spatially and temporally continuous representations of available weather observations worldwide. The key difference between individual observational data streams and reanalysis is that the latter methodology relies on sophisticated weather/ocean modeling systems; it is unfeasible to precisely and accurately measure the Earth system on a routine basis everywhere, so the modeling component of reanalysis extends local observations to unresolved areas in a way that is constrained by the known laws of physics (see Sec. 2 of Dee et al., 2011). As an example, reanalysis systems ingest observations from sea-surface altimeters on satellites over remote oceanic regions and thereby incorporate approximate representations of the interplay between ocean waves and the overlying atmosphere, as it contributes to local wind turbulence and wind gustiness.

The reanalysis process can be described by first collating available weather/ocean observations in a 12-hour interval prior to analysis time. Next, the process minimizes the apparent difference between the aforementioned observations and a modeled approximation of background environmental conditions. Finally, the model is integrated forward to repeat the process for a subsequent analysis cycle. One additional strength of reanalysis products is that they reproduce the available observational record, worldwide, using a consistent model version across all years of the data record. (Information about the latest version of the ECMWF Integrated Forecast System can be accessed online via, https://www.ecmwf.int/en/forecasts/datasets/archive-datasets/reanalysis-datasets/era-interim.)

Data from ERAi are available from January 1, 1979 to present, worldwide, and at six-hour analysis intervals (Berrisford et al., 2011). Output from the ERAi model can be obtained in a variety of spatial resolutions to support different applications. For the purpose of this study, native ERAi data were chosen at a spatial resolution of 1.0° to match available fuel consumption and chemical emissions inventories. The resulting geographic grid has dimensions of 181 points in latitude and 360 points in longitude. Data are available at the surface level as well as at various altitudes above the surface corresponding to standard reporting atmospheric pressures between 1000.0 and 1.0 hectopascals (hPa; for reference, 1.0 hPa is equivalent to 1.0 millibar for atmospheric pressure).

The variables used here are surface pressure (P_{sfc}), which is an input to the air lubrication methodology, zonal wind (u; the wind component in the east-west direction), meridional wind (v; the wind component in the north-south direction), temperature (T), geopotential height (ϕ, i.e., approximately equal to the product of gravity, g, and altitude, z) and relative humidity (RH, i.e., the amount of water vapor present, expressed as a fraction of the total amount that the air can hold at the local temperature). Analysis-only

(i.e., non-forecast) values were chosen at 0:00, 6:00, 12:00 and 18:00 universal time (UTC), in adherence to standard meteorological reporting time conventions, for both surface and pressure-level datasets and all calendar dates spanning January 1, 2015 to December 31, 2015 (the data are accessible online via, https://apps.ecmwf.int/datasets/.data/interim-full-daily/levtype=sfc/; the pressure-level data are accessible online via, https://apps.ecmwf.int/datasets/data/interim-full-daily/levtype=pl/).

The specified reference heights for this analysis were near-surface, 20, 30, 80, 100, 250 and 500 m mean-sea-level (MSL) altitude. The native ERAi data above the surface, given in terms of pressure, need to be transformed to height coordinates. Ignoring small corrections to the gravitational force and assuming that the atmospheric pressure at any point is the sum of the weight from over-lying air up to the top of the atmosphere, the local MSL altitude of a given reanalysis data point can be found by taking the quotient of the local geopotential height of the pressure surface (ϕ, which has units of m^2 s^{-2}) and gravity, g. Because the relationship between pressure and altitude is not systematically one-to-one, this operation needs to be carried out at every single point in the grid above the surface, taking local thermodynamic conditions in the atmosphere into account. ERAi data used here were captured at nominal atmospheric pressures of 1000, 975, 950, 925, 900, 875 and 850 hPa above each geolocated gridpoint prior to converting into local MSL height.

After transforming the vertical data coordinate from pressure to MSL height, the next step consisted of linear data interpolation for each variable, u, v, RH, and T, to the specified reference heights above the surface. The ERAi reanalysis involves complex theoretical methods to infer/extrapolate quantities like wind speed, temperature and moisture content throughout the vertical atmospheric column, especially close to the surface where conditions can be very turbulent. Previous investigators have found that simplified data interpolation approaches (i.e., vertical linear interpolation) to match various reference heights does not significantly contribute to errors in analysis that follows (e.g., Decker et al., 2012). Therefore, a vertical profile of each reanalysis variable was constructed using source altitudes at every location spanning a geographic grid of points—that is, with dimensions of 181, 360—prior to calculating the vertical linear interpolation to reference heights needed for this study. It is important to note that the vertical interval of reference altitudes chosen here is comparable to the vertical resolution of the source reanaly-sis data, to represent the input data as closely as possible.

Following the interpolation step, diagnostic quantities of true wind speed (V_t) and true wind direction (γ) were calculated from the source reanalysis data. The meteorological reporting convention for wind speed and direction is in accordance with the direction that the wind originates from. The following formulas convert cartesian vector components, i.e., u and v representing east-west and north-south directions respectively, to the normal reporting convention:

$$V_t = \sqrt{u^2 + v^2}$$

$$\gamma = 270.0 - \left(arctan2(v,u) \times \frac{180.0}{\pi} \right)$$

Wind direction utilizes the two-argument arc-tangent function that is included in standard libraries of common coding languages (see https://www.eol.ucar.edu/content/wind-direction-quick-reference). In the rotor sail methodology, we use the 30 m MSL altitude values for wind speed and direction as a proxy for the actual wind speed and direction the rotor sail would encounter. The air lubrication methodology uses surface pressure as an input variable.
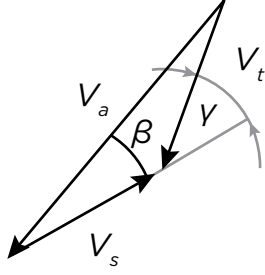
ROTOR SAILS

We estimated fuel, CO_2, and carbon-intensity savings from rotor sails in five steps:

Step 1	Find the apparent wind speed by combining ship speed and wind speed
Step 2	Find the lift and drag forces produced by rotors
Step 3	Find the thrust force and power produced by rotors
Step 4	Find the power consumed by rotors
Step 5	Find the net power saving by hour for each ship (equivalent to fuel and CO_2 savings, which are also equivalent to carbon-intensity reductions)

1. Find the apparent wind speed by combining ship speed and wind speed

The apparent wind speed, V_a, depends on both true wind speed, V_t, and ship speed, V_s. The relationship is shown in Figure A1, where γ is the true wind direction from the meteorological data and β is the is the apparent wind direction.

Figure A1. Correlation among ship speed, wind speed, and apparent wind speed. Picture adapted from Lele and Rao (2016).

Given that rotor sails operate near the surface, we take the wind speed and direction at 30 m as a proxy for the wind speed and direction that the rotor sail would encounter.

The apparent wind speed V_a and the apparent wind direction β can be calculated as,

$$V_a = \sqrt{V_t + V_s^2 - 2V_tV_s\cos(\gamma)}$$

$$\beta = \cos^{-1}\left(\frac{V_t^2 - V_a^2 + V_s^2}{-2V_aV_s}\right)$$

Where

V$_t$ is the true wind speed (unit: m s^{-1})

V$_s$ is the ship speed (unit: m s^{-1})

γ is the true wind direction (unit: degree)

2. Find the lift and drag forces produced by rotors

The lift and drag forces produced by rotors can be represented as L and D (units: N), which are found by

$$L = p_o \times A_r \times C_L$$

$$D = p_o \times A_r \times C_D$$

Where

p$_o$ is the stagnation pressure (unit: Pa)

A$_r$ is the surface area of the rotor (unit: m^2)

C$_L$ is the three-dimensional lift coefficient, which is assumed to be 12.5 (Craft et al., 2012)

C$_D$ is the three-dimensional drag coefficient, which is assumed to be 0.2 (Craft et al., 2012)

The stagnation pressure p$_o$ (unit: Pa) can be found by,

$$p_o = \frac{\rho_A \times V_a^2}{2}$$

Where

ρ_A is the density of air (unit: kg m^{-3}) at a certain height, accounting for local water vapor content of the air.

V$_a$ is the apparent wind speed (unit: m s^{-1})

Thus, ρ_A is estimated by following steps:

- Find the saturation vapor pressure, e$_{sat}$
- Find the actual vapor pressure, e$_{wet}$,
- Find the dry air pressure e$_{dry}$
- Find ρ_A by combining both vapor pressure and dry air pressure

The saturation vapor pressure, e$_{sat}$, is a function of temperature only (Bolton, 1980), which is approximated as:

$$e_{sat} = 6.112 \times \exp\left(\frac{17.67 \times T}{T + 243.5}\right)$$

Where

T is the instantaneous, local air temperature at a certain height (unit: K) (from met. data)

The actual vapor pressure, e$_{wet}$, is found by multiplying the saturation vapor pressure e$_{sat}$ and the relative humidity (RH):

$$e_{wet} = e_{sat} \times RH$$

Where

e$_{sat}$ is the saturation vapor pressure (unit: Pa)

RH is the relative humidity at a certain height (unit: %) (from met. data)

The dry air pressure e_{dry} (unit: Pa) can be found as

$$e_{dry} = p_s \times e_{wet}$$

Where

p_s is the total air pressure at a certain height (unit: Pa) (from met. data)

e_{wet} is the actual vapor pressure (unit: Pa)

The density of air, ρ_A, can be estimated by combining both vapor pressure and dry air pressure:

$$\rho_A = \frac{e_{dry}}{287 \times T} + \frac{e_{wet}}{465 \times T}$$

Where

e_{dry} is the dry air pressure (unit: Pa)

e_{wet} is the actual vapor pressure (unit: Pa)

T is the instantaneous local air temperature at a certain height (unit: K) (from met. data)

The surface area of a rotor, A_r (unit: m2), can be calculated as:

$$A_r = \pi \times d \times h$$

Where

d is the diameter of rotors (unit: m)

h is the height of rotors (unit: m)

3. Find the thrust force and power produced by rotors

We later projected the lift (L) and drag (D) forces to the force in ship moving direction (F_X) and the force perpendicular to the ship (F_Y), as shown below:

$$\begin{bmatrix} F_X \\ F_Y \end{bmatrix} = \begin{bmatrix} \cos\beta & \sin\beta \\ -\sin\beta & \cos\beta \end{bmatrix} \times \begin{bmatrix} -D \\ L \end{bmatrix}$$

which can be also written as:

$$F_X = L \sin \beta - D \cos \beta$$

The force in the ship moving direction, F_X, is also known as the thrust force, which is the main contribution from rotors that can eventually provide the extra propulsive power for ships to save the energy use. The generated propulsive power, P_{gen} (unit: W), is the product of thrust force and ship speed, which can be calculated as,

$$P_{gen} = F_X \times V_s$$

Where

F_X is the thrust force (unit: N)

V_s is the ship speed (unit: m s^{-1})

4. Find the power consumed by rotors

The resistive force and rotational energy (power) required to overcome this resistance due to skin friction is estimated by using the flat plate boundary layer theory (Lele & Rao, 2016). The frictional coefficient c_f is decided by the Reynolds number Re, and Re and c_f are calculated as:

$$Re = \frac{\rho_A \times C_{rot} \times V_a \times L_{Re}}{\mu}$$

$$C_f = \frac{0.455}{(\log Re)^{2.58}} - \frac{1700}{Re}$$

Where

ρ_A is the density of air (unit: kg m^{-3})

C_{rot} is the coefficient between the rotational speed of rotor U_{rot} and the apparent wind speed V_a, which is assumed to be 5 in this study (Lele & Rao, 2016)

V_a is the apparent wind speed (unit: m s^{-1})

μ is the dynamic viscosity of air (unit: Pa*s)

L_{Re} is the characteristic length (unit: m) i.e. circumference of rotor, which is simply π times the diameter of the rotor.

The dynamic viscosity of air, μ (unit: Pa*s), is estimated by the Sutherland's law (Sutherland, 1893), as shown in the equation below:

$$\mu = \frac{C_1 \times T^{\frac{2}{3}}}{T + S}$$

Where

C_1 is the Sutherland's law constant equals to 1.458 *10^{-6} (unit: kg m^{-1} s^{-1} K$^{-1/2}$)

T is the instantaneous air temperature at a certain height (unit: K) (from met. data)

S is the Sutherland temperature assumed to be 110.4 (unit: K)

After we find the c_f, we can then calculate the frictional force F_f from the rotor rotation as,

$$F_f = C_f \times \rho_A \times \frac{U_{rot}^2}{2} \times A_r$$

Where

c_f is the frictional coefficient of the rotor obtained from above

ρ_A is the density of air (unit: kg m^{-3})

A_r is the surface area of the rotor (unit: m^2), and

U_{rot} is the rotational speed of the rotor (unit: m s^{-1}), which can be calculated as:

$$U_{rot} = C_{rot} \times V_a$$

Where

C_{rot} is the coefficient between U_{rot} and V_a, which is assumed to be 5 (Lele & Rao, 2016)

V_a is the apparent wind speed (unit: m s^{-1}).

Finally, the power required to rotate the rotor, P_{con} (unit: W), is calculated as:

$$P_{con} = F_f \times U_{rot}$$

Where

F_f is the frictional force from the rotor rotation (unit: N)

U_{rot} is the rotational speed of the rotor (unit: m s^{-1})

5. Find power savings by hour for each ship (equivalent to fuel savings)

According to De Marco et al. (2016), the contribution from rotors would be expected to increase almost linearly with the number of devices installed on the same ship. Thus, the net power output from rotors, P_{net} (unit: W), is calculated as:

$$P_{net} = (P_{gen} - P_{con}) \times Num_{rot} \times \eta_{prop}$$

Where

P_{gen} is the power generated by rotors every hour (unit: W)

P_{con} is the power consumed by rotors every hour (unit: W)

Num_{rot} is the number of rotors

η_{prop} is the ship propulsion efficiency assumed to be 0.75 (MAN Energy Solutions, n.d.)

To calculate power savings for each ship for every hour (t), we first lookup estimated main engine power demand (P_{ME}) for that ship along each modeled route based on the global ship emissions inventory reported in Olmer, Comer, Roy, Mao, and Rutherford (2017). To find the power savings (P_s), in percent, at every hour, we divide P_{net} by P_{ME}:

$$P_{s,t} = \frac{P_{net,t}}{P_{ME,t}} = F_{s,t}$$

Fuel savings (F_s), in percent, are equivalent to P_s at every hour, t. Multiplying F_s by fuel consumption (F_c) for every hour results in hourly fuel consumption reductions from using rotor sails. Summing up F_c for every hour t of a route gives route-level fuel consumption savings that are directly proportional to route-level CO_2 and carbon-intensity reductions.

AIR LUBRICATION

To estimate the fuel, CO_2, and carbon-intensity savings for air lubrication, we adapted the methodology of Mäkiharju, Perlin, and Ceccio (2012).

According to Mäkiharju et al., the percent of energy saved, %E_{saved}, is estimated as,

$$\%E_{saved} = f_{FD} \times \frac{A_{ac}}{A_{wet}} \times \%D_R - \frac{P_{comp} \times \eta_{prop}}{P_D \times \eta_{elec}}$$

Where

f_{FD} is the fraction of frictional drag of total resistance (unit: %)

A_{ac}/A_{wet} is the wetted area covered by air divided by the total wetted hull area

$\%D_R$ is the frictional drag reduction on areas with air lubrication (unit: %)

P_{comp} is the power used by air compressor (unit: W)

P_{ME} is the power demand for ship main engine (unit: W)

η_{prop} is the propulsive efficiency (unit: %)

η_{elec} is the electrical generating efficiency (unit: %)

Compared to the rotor sail, the MALS system has fewer real-world applications and fewer studies of performance have been conducted to date; therefore, we made assumptions based on the existing literature and the ships that we modeled (Table A). This study estimates the fuel saving by MALS as follows:

Step 1   Find the main engine power reduced by MALS

Step 2   Find the auxiliary power consumed by MALS

Step 3   Find the net power saved by MALS (equivalent to fuel and CO_2 savings, which are also equivalent to carbon-intensity reductions)

1. Find the main engine power reduced by MALS

The ICCT has estimated the main engine power use for each ship, at each hour, from the SAVE model (Olmer et al., 2017), which is equivalent to the hourly propulsive power. Thus, the main engine power reduction by MALS, P_{red} (unit: W), is considered as the benefit from the ship drag reduction, which could be shown as:

$$P_{red} = P_{ME} \times LF \times f_{FD} \times \frac{A_{ac}}{A_{wet}} \times \%D_R$$

Where

P_{ME} is the power demand for ship main engine (unit: W)

LF is the main engine load factor (unit: %; from ICCT data that underlies Olmer et al. [2017])

f_{FD} is the fraction of frictional drag of total resistance (unit: %; see Table A)

A_{ac}/A_{wet} is the wetted area covered by air divided by the total wetted hull area (see Table A)

$\%D_R$ = frictional drag reduction on areas with air lubrication (unit: %; see Table A)

2. Find the auxiliary power consumed by MALS

The auxiliary power consumed by MALS, P_{con} (unit: W), arises from the power p used by the air compressor P_{comp}, as shown in the equation below:

$$P_{con} = \frac{P_{comp}}{\eta_{elec}}$$

And the power used by the air compressor, P_{comp} (unit: W), is calculated as follows:

$$P_{comp} = \frac{\dot{m}_g \times P_1 \times n}{\eta_c \times \rho_{g,1} \times (n-1)} \times \left(\left[\frac{p_3 \times \Delta p_{loss}}{p_1} \right]^{\frac{n-1}{n}} -1 \right)$$

Where

$\dot{m}_g$ is the mass flow rate of gas (see equation below) (unit: kg s^{-1})

p_1 is the surface pressure, which varies (unit: Pa)

n is the polytropic index (see Table A)

p_3 is the hydrostatic pressure at the draught depth (unit: Pa)

Δp_{loss} is the pressure loss through piping and other minor losses and is defined below (unit: Pa)

η_c is the efficiency of the compressor (see Table A)

$\rho_{g,1}$ is the density of the nitrogen gas to be compressed, which is 1.165 kg/m³ (unit: kg m^{-3})

η_{elec} is the electrical generating efficiency (unit: %; see Table A)

The mass flow rate of gas $\dot{m}_g$ (Unit: kg s$_{-1}$) depends on the volumetric gas flux, the density of gas (assumed to be nitrogen gas), the surface pressure, and the pressure at depth, which can be expressed as,

$$\dot{m}_g = Q \times \frac{\rho_{g,1} \times p_3}{p_1}$$

And

$$Q = t \times B \times U$$

Table A: Assumptions for the hull air lubrication system analysis

Assumption	Description	Unit	Value	Source
f_{FD}	Fraction of frictional drag of total resistance	%	60%	Jang et al. (2014)
A_c/A_{wet}	Wetted area covered by air divided by the total wetted hull area	%	45%	Mäkiharju et al. (2012) suggested 50% and Jang et al. suggested 42.5%; this study then splits the difference at 45%.
%DR	Frictional drag reduction on areas with air lubrication	%	60%	Based on NMRI presentation slide 6 and Kawakita et al (2015)
Pipe surface roughness	Pipe surface roughness	mm	0.07	Mäkiharju et al. (2012)
η_c	Efficiency of the compressor	%	60%	Mäkiharju et al. (2012)
η_{elec}	Electrical generating efficiency	%	90%	Mäkiharju et al. (2012)
n	Polytropic index		1.4	Mäkiharju et al. (2012)
ΣK	Minor loss coefficient in piping		5	Mäkiharju et al. (2012)
L_{pipe}	Length of pipe	m	64	Mitsubishi Heavy Industries (2013)
d_{pipe}	Diameter of pipe	m	0.15	Mäkiharju et al. (2012)
t	Thickness of air layer	mm	7	Monohakobi Technology Institute (2012)

Where

Q is the volumetric gas flux (unit: $m^3 \ s^{-1}$)

$\rho_{g,1}$ is the density of the gas to be compressed (unit: kg m^{-3})

p_3 is the hydrostatic pressure at the draught depth and is defined below (unit:Pa)

p_1 is the surface pressure which varies (unit: Pa)

t is the thickness of air layer (unit: m) (see Table A)

B is the width of the air lubricated region, assumed to be the breadth of the ship (unit: m).

U is the free-stream speed, estimated by the speed over ground of the ship (unit: m s^{-1})

The hydrostatic pressure at the draught depth (p_3) (unit: Pa) is calculated as:

$$p_3 = \rho_{sw} \times g \times D + p_1$$

Where

ρ_{sw} = Density of the seawater (unit: kg m^{-3}), assuming constant average salinity of 25.0 g kg^{-1} and following the empirical formulation of Millero and Poisson (1981).

g = Gravitational acceleartion (unit: m s^{-2})

D = Ship draught (unit: m)

p_1 = Surface pressure, which varies (unit: Pa)

Pressure loss through piping and other minor losses (Δp_{loss}) (unit: Pa), can be found by,

$$\Delta p_{loss} = \frac{\rho_{g,3} \times U^2}{2} \times \left(\frac{f \times L_{pipe}}{d_{pipe}} + \sum K \right)$$

Where

$\rho_{g,3}$ is the density of the compressed gas at p_3 (unit: kg m^{-3})

U is the free-stream speed, estimated by the speed over ground of the ship (unit: m s^{-1})

f is the friction factor calculated based on the Moody chart with the assumed pipe surface roughness (see Table A)

L_{pipe} is the length of air pipes (unit: m; see Table A)

d_{pipe} is the diameter of air pipes (unit: m; see Table A)

ΣK is the minor loss coefficient in piping (see Table A)

3. Find the net power saved by MALS (equivalent to fuel saving)

Finally, we can calculate the hourly net power saving ($P_{net,t}$) from MALS by subtracting the consumed auxiliary power at hour t ($P_{con, t}$) from the reduced main engine power at time t ($P_{red, t}$).

$$P_{net,t} = P_{red,t} - P_{con,t}$$

To calculate power savings for each ship for every hour (t), we first look up estimated main engine power demand (P_{ME}) for that ship along each modeled route based on the global ship emissions inventory reported in Olmer et al. (2017). To find the power savings (P_s), in percent, at every hour, we divide P_{net} by P_{ME}:

$$P_{s,t} = \frac{P_{net,t}}{P_{ME,t}} = F_{s,t}$$

Fuel savings (F_s), in percent, are equivalent to P_s at every hour t. Multiplying F_s by fuel consumption (F_c) for every hour results in hourly fuel consumption reductions from using MALS. Summing up F_c for every hour t of a route gives route-level fuel consumption savings that are directly proportional to route-level CO_2 and carbon-intensity reductions.

References for Appendix

Bolton, D. (1980). The computation of equivalent potential temperature. *Monthly Weather Review, 108*(7), 1046–1053. https://doi.org/10.1175/1520-0493(1980)108<1046:TCOEPT>2.0.CO;2.

Craft, T. J., Iacovides, H., Johnson, N., & Launder, B. E. (2012). Back to the future: Flettner-Thom rotors for maritime propulsion? In *Proceeding of THMT-12. Proceedings of the Seventh International Symposium On Turbulence, Heat and Mass Transfer Palermo, Italy, 24-27 September, 2012* (p. 10). Antalya, Turkey: Begellhouse. https://doi.org/10.1615/ICHMT.2012.ProcSevIntSympTurbHeatTransfPal.1150.

Decker, M., Brunke, M.A., Wang, Z., Sakaguchi, K., Zeng, X., & Bosilovich, M.G. (2012). Evaluation of the reanalysis products from GSFC, NCEP, and ECMWF using flux tower observations. *Journal of Climate, 25*(6), 1916–1944. https://doi.org/10.1175/JCLI-D-11-00004.1.

Dee, D., Fasullo, J., Shea, D., Walsh, J. (2016). The climate data guide: Atmospheric reanalysis: overview & comparison tables. National Center for Atmospheric Research (Boulder, CO.). Retrieved from: https://climatedataguide.ucar.edu/climate-data/atmospheric-reanalysis-overview-comparison-tables.

Dee, D., Uppala, S., Simmons, A., Berrisford, P., Poli, P., Kobayashi, S., . . . & Vitart, F. (2011). The ERA-Interim reanalysis: Configuration and performance of the data assimilation system. *Quarterly Journal of the Royal Meteorological Society, 137*(656), 553–597. https://doi.org/10.1002/qj.828.

De Marco, S. Mancini, C. Pensa, G. Calise, and F. De Luca. (2016). Flettner rotor concept for marine applications: A systematic study. *International Journal of Rotating Machinery*, 2016. https://doi.org/10.1155/2016/3458750.

Jang, J., Choi, S. H., Ahn, S.-M., Kim, B., & Seo, J. S. (2014). Experimental investigation of frictional resistance reduction with air layer on the hull bottom of a ship. *International Journal of Naval Architecture and Ocean Engineering, 6*(2), 363–379. https://doi.org/10.2478/IJNAOE-2013-0185.

Kawakita, C., Sato, S., & Okimoto, T. (2015). Application of simulation technology to Mitsubishi Air Lubrication System. *Mitsubishi Heavy Industries Technical Review, 52*(1), 50–56. Retrieved from: https://www.mhi.co.jp/technology/review/pdf/e521/e521050.pdf.

Lele, A. & Rao, K. V. S. (2016). Ship propulsion strategies by using wind energy. In *2016 International Conference on Emerging Technological Trends (ICETT)* (pp. 1–6). https://doi.org/10.1109/ICETT.2016.7873693.

Mäkiharju, S. A., Perlin, M., & Ceccio, S. L. (2012). On the energy economics of air lubrication drag reduction. *International Journal of Naval Architecture and Ocean Engineering, 4*(4), 412–422. https://doi.org/10.2478/IJNAOE-2013-0107.

MAN Energy Solutions. (n.d.). Basic principles of propulsion of ship propulsion. Retrieved from https://marine.man-es.com/propeller-aft-ship/basic-principles-of-propulsion.

Millero, F. J., & Poisson, A. (1981). International one-atmosphere equation of state of seawater. *Deep Sea Research Part A, Oceanographic Research Papers*, *28*(6), 625–629. https://doi.org/10.1016/0198-0149(81)90122-9.

Mizokami, S., Kawakita, C., Kodan, Y., Takano, S., Higasa, S., & Shigenaga, R. (2010). Experimental study of air lubrication method and verification of effects on actual hull by means of sea trial. *Mitsubishi Heavy Industries Technical Review, 47*(3), 41–47. Retrieved from https://www.mhi.co.jp/technology/review/pdf/e473/e473041.pdf.

Olmer, N., Comer, B., Roy, B., Mao, X., & Rutherford, D. (2017). *Greenhouse gas emissions from global shipping, 2013–2015.* The International Council on Clean Transportation. Retrieved from: https://www.theicct.org/publications/GHG-emissions-global-shipping-2013-2015.

Sutherland, W. (1893). The viscosity of gases and molecular force. *The London, Edinburgh, and Dublin Philosophical Magazine and Journal of Science, 36*(223), 507–531.